

# Damping Scaling Factors for Vertical Elastic Response Spectra for Shallow Crustal Earthquakes in Active Tectonic Regions

Sanaz Rezaeian,<sup>a)</sup> Yousef Bozorgnia,<sup>b)</sup> I. M. Idriss,<sup>c)</sup>  
Norman A. Abrahamson,<sup>d)</sup> Kenneth W. Campbell,<sup>e)</sup> and Walter J. Silva<sup>f)</sup>

This paper develops a new model for a damping scaling factor (DSF) that can be used to adjust elastic response spectral ordinates for the vertical component of earthquake ground motion at a 5% viscous damping ratio to ordinates at damping ratios between 0.5% and 30%. Using the extensive NGA-West2 database of recorded ground motions from worldwide shallow crustal earthquakes in active tectonic regions, a functional form for the median DSF is proposed that depends on the damping ratio, spectral period, earthquake magnitude, and distance. Standard deviation is a function of the damping ratio and spectral period. The proposed model is compared to the DSF for the “average” horizontal component. In general, the peak in DSF is shifted toward shorter periods and is farther from unity for the vertical component. Also, the standard deviation of DSF for vertical motion is slightly higher than that observed for the “average” horizontal component. [DOI: 10.1193/100512EQS299M]

## INTRODUCTION

The current practice of seismic design is primarily based on the effects of horizontal components of ground motion on structures. However, the effects of the vertical component of ground motion can be important for certain types of structures and for nonstructural components. For example, bridges, diaphragms, cantilever and base-isolated structures can be sensitive to the vertical excitation. In the design of structures that house sensitive equipment or anchorages for nonstructural components the vertical ground shaking can be influential, especially for sites close to active faults. Furthermore, some structural components and systems can have short vertical natural periods that are not far from the dominant period of vertical input motion (see, e.g., [Bozorgnia et al. 1998](#)); thus, in-structure amplification of vertical acceleration is expected.

---

<sup>a)</sup> U.S. Geological Survey, Golden, CO, [sanazr128@yahoo.com](mailto:sanazr128@yahoo.com)

<sup>b)</sup> Pacific Earthquake Engineering Research Center, University of California, Berkeley, CA

<sup>c)</sup> University of California, Davis, CA

<sup>d)</sup> Pacific Gas & Electric Company, CA

<sup>e)</sup> EQECAT Inc., Oakland, CA

<sup>f)</sup> Pacific Engineering & Analysis, El Cerrito, CA

## VERTICAL GROUND MOTION PREDICTION EQUATIONS

To analyze the effects of earthquake ground motions on structures, ground motion prediction equations (GMPEs) are often used in practice to estimate the intensity of ground shaking in the form of elastic response spectral values. Many GMPEs have been developed for the horizontal ground motion. For example, the next generation attenuation (NGA) relations provided GMPEs for the “average” horizontal component (Power et al. 2008). On the contrary, very few GMPEs have been developed for the vertical ground motion component. Traditionally, seismic design guidelines have used a constant, period-independent, spectral ratio of 2/3 to scale the horizontal response spectrum to the vertical response spectrum (e.g., Section 1.6.1.5.2 of FEMA 356 2000). However, it is now well-established that at short periods and in near-source areas, the vertical response spectrum can exceed its horizontal counterpart. Thus, the traditional 2/3 scaling of the horizontal spectrum can significantly underestimate the vertical ground motion, or conversely, at long periods the 2/3 rule could be rather conservative (e.g., Campbell 1985, Niazi and Bozorgnia 1991, 1992, Bozorgnia et al. 1995, Silva 1997, McGuire et al. 2001, Bozorgnia and Campbell 2004, BSSC 2009).

Several GMPEs have been developed for the vertical response spectra or for the vertical-to-horizontal (V/H) response spectral ratios (e.g., Abrahamson and Silva 1997, Campbell 1997, Sadigh et al. 1997, Campbell and Bozorgnia 2003, Gülerce and Abrahamson 2011). The vertical model by Campbell and Bozorgnia (2003) was later simplified for design purposes in Bozorgnia and Campbell (2004) and became the basis for developing vertical design spectra in the 2009 National Earthquake Hazards Reduction Program (NEHRP) provisions (BSSC 2009). A few other investigators have also proposed models for developing a vertical design spectrum (e.g., Elnashai and Papazoglu 1997, Malhotra 2006). Only in recent years have building codes started to provide guidelines on developing a vertical design spectrum based on a more meaningful ratio than 2/3 or even completely independent of the horizontal design spectrum (i.e., CEN 2004 and BSSC 2009). Bommer et al. (2011) have developed a model for the V/H response spectral ratio for Europe and the Middle East. Tezcan and Piolatto (2012) have proposed a probabilistic nonparametric model for the V/H ratio that does not require a functional form and treats the model coefficients as random variables.

## DAMPING SCALING OF THE VERTICAL RESPONSE SPECTRUM

Historically, GMPEs for both horizontal and vertical ground motions have been developed at a 5% reference damping ratio (i.e., the equivalent viscous damping ratio of the system is 5% of critical; Chopra 2012). In reality, the damping ratio, which represents the level of energy dissipation in structural, geotechnical, and nonstructural systems, can be different from 5% depending on the structural type, construction material, and level of ground shaking (for examples, see Rezaeian et al. 2012). In a previous paper, we presented an empirically developed predictive model for a damping scaling factor (DSF) for the “average” horizontal component (Rezaeian et al. 2014). The DSF was used to scale pseudo-response spectral accelerations (PSA) at a 5% damping ratio to PSA at other damping ratios. The “average” horizontal component, which hereafter will simply be referred to as the horizontal component, was represented in two ways: (1) GMRotI50 horizontal component, as defined by

Boore et al. (2006) and used in the NGA GMPEs; and (2) RotD50 horizontal component as defined by Boore (2010) and used in the update of the NGA GMPEs (i.e., NGA-West2; see Bozorgnia et al. 2012). These two components are independent of the in situ orientation of a seismometer. The DSFs of these two components had the same functional forms, but different model coefficients, and only minor differences between them. In this paper, we extend the DSF model to the vertical component of ground motion.

In the past two decades, a large number of studies have been conducted on damping scaling of the response spectrum. A comprehensive summary of the literature is given in the report by Rezaeian et al. (2012). The majority of these studies focus on damping scaling factors for the horizontal ground motion. Very few have developed damping scaling factors for the vertical component. Mohraz (1976) used 54 recordings from 16 earthquakes to study the vertical response spectrum at five damping ratios: 0%, 2%, 5%, 10%, and 20%. Trifunac and Lee (1989) used a database of 438 recordings from 104 earthquakes, mostly from California, to develop GMPEs for the vertical pseudo-velocity response spectrum at 0%, 2%, 5%, 10%, and 20% damping ratios. Berge-Thierry et al. (2003) used 485 recordings mainly from European earthquakes supplemented by a few California events to develop GMPEs for the vertical pseudo-acceleration response spectrum. Their model coefficients were computed for 5%, 7%, 10%, and 20% damping ratios. A disadvantage of developing GMPEs at multiple levels of damping is that the resulting models cannot be directly used to adjust other existing or updated 5% damped GMPEs. However, scaling factors for transition from 5% to other damping ratios can be estimated from these models for any combination of their predictor variables and can be interpolated between the discrete damping ratios covered by the original GMPE.

An alternative approach taken by most researchers, dating back to the classic work of Newmark and Hall (1982) and also used in Rezaeian et al. (2014), is to develop models of multiplicative factors (i.e., DSF) that scale the 5% damped spectral ordinates predicted by any GMPE to ordinates for other damping ratios. The advantages of this approach are that it does not require interpolation between discrete damping ratios and can be easily applied to GMPEs other than those from which the model was derived. Models for the DSF of vertical ground motion have been proposed by McGuire et al. (2001) based on random vibration theory and by Abrahamson and Silva (1996) based on empirical analyses. The procedure recommended by McGuire et al. (2001) is applicable for damping ratios between 0.5% to 20% and uses similar functional forms for the horizontal and vertical ground motions. Their DSF model depends on the damping ratio, spectral period, and duration of motion. Abrahamson and Silva (1996) proposed a model for  $\ln(DSF)$  of the vertical ground motion that is a function of earthquake magnitude. Their model coefficients are given at specified damping ratios (between 0.5% and 20%) and spectral periods (between 0.02 s and 5 s). Finally, Malhotra (2006) used recorded data to develop functional forms for the DSF of a smooth vertical response spectrum. Different functions are given for the acceleration-constant, velocity-constant, and displacement-constant regions of the smooth spectrum.

In this study, we use an extensive database of over 2,000 recordings from shallow crustal events in active tectonic regions to develop a new DSF model for the vertical component of ground motion. Our database is a subset of the database developed for the NGA-West2

project, which is a research program coordinated by the Pacific Earthquake Engineering Research Center (PEER) to update the 2008 NGA models (Ancheta et al. 2013). It should be noted that the new DSF model is not dependent on the NGA GMPEs, or any other specific GMPE, as this model is developed directly from the spectral ordinates of the recorded data. Therefore, the model is general enough to be applicable to a wide range of GMPEs for vertical elastic response spectra.

## CHARACTERISTICS OF THE VERTICAL GROUND MOTION

In this paper, we also highlight the differences between the DSF of vertical and horizontal ground motions. These differences could be due to the specific characteristics of the vertical component of ground motion. Several investigators have studied the characteristics of the vertical ground motion (see details in Bozorgnia and Bertero 2004, Bozorgnia and Campbell 2004, Malhotra 2006, and Aoi 2008). In particular, the vertical component is richer in high-frequency content than the horizontal component. This causes higher vertical response spectral ordinates at shorter periods as compared to horizontal spectra. This difference increases with decreasing soil stiffness. Another major difference is that the vertical component attenuates at a higher rate than the horizontal component. As a result, generally the V/H ratio has been found to be a strong function of natural period, source-to-site distance, and local site conditions, and a weaker function of other variables such as earthquake magnitude and faulting mechanism (e.g., Bozorgnia and Campbell 2004). Malhotra (2006) observed a much smaller normalized (as defined in Malhotra 2006) peak ground velocity, PGV, for the vertical motion relative to that of the horizontal motion. Since spectral acceleration in mid-range periods (about 0.3 s to 2 s) is highly correlated with PGV, one can expect lower V/H ratios in this range. Aoi et al. (2008) studied vertical motions from the 2008 Iwate-Miyagi earthquake in Japan. In addition to the large amplitudes of the vertical component relative to the horizontal, they observed a distinct asymmetry around the zero line in vertical acceleration time series. They explained this phenomenon for extreme ground motions by a simple model of a mass bouncing on a trampoline.

Some seismological explanations have been offered in the literature for the differences observed between the vertical and horizontal ground motions. The conversion of SV-waves to compressional P-waves at the rock/soil interface and their refraction into a more vertical angle as the seismic waves propagate toward a site can be a contributing factor (Silva 1997). This S-to-P wave conversion can explain the high-amplitude, high-frequency nature of near-source vertical accelerations (Amirbekian and Bolt 1998). Beresnev et al. (2002) suggested that vertical ground motions are dominated by SV-waves at longer periods and that P-waves could be significant contributors at shorter periods, possibly influencing the characteristics of the vertical ground motion. In this paper, we also observe systematic, period-dependent differences between the DSF of vertical and horizontal ground motions.

In the following, we first describe the database of strong ground motion records that is used in this study for empirical modeling. Then, a summary of the observed dependencies between the DSF and potential predictor variables is presented. Next, models for the median DSF and its logarithmic standard deviation for the vertical component of ground motion are proposed. Finally, the model is compared to that of the horizontal ground motion.

## VERTICAL GROUND MOTION DATABASE

Rezaeian et al. (2014) used a subset of the NGA-West2 database of recorded ground motions with moderate to large magnitude events to develop models for damping scaling of horizontal components, that is, GMRotI50 and RotD50 components. This database was summarized in detail in Rezaeian et al. (2014). For the present paper, the elastic response spectra for the available vertical components of the same records have been calculated at the same 11 damping ratios:  $\beta = 0.5\%$ , 1%, 2%, 3%, 5%, 7%, 10%, 15%, 20%, 25%, and 30%.

As described in Rezaeian et al. (2014), we select records with closest distance to rupture,  $R_{RUP}$ , of less than 50 km for empirical modeling. This is to ensure a proper model for near-source data. The validity of the model for distances beyond 50 km is later verified by examining the residuals for the remaining records. The selected database contains 2,229 vertical components from 218 earthquakes. Vertical components were not available for 21 records in the database used by Rezaeian et al. (2014; i.e., 2,250 horizontal components).

In our selected database, the moment magnitude  $M$  ranges between 4.2 and 7.9, with a mean of about 6.1. The distance  $R_{RUP}$  varies between 0.05 km and 49.97 km, with a mean of about 27 km. The magnitude-distance distribution is shown in Figure 1. To examine the effects of site conditions and duration of motion on damping scaling, we use  $V_{S30}$  and  $D_{5-75}$ , respectively.  $V_{S30}$  represents the time-averaged shear wave velocity in the top 30 m of the site. This measure varies between 116 m/s and 2,016 m/s, with a mean of about 397 m/s.  $D_{5-75}$  represents the significant duration of motion measured from 5% to 75% of Arias intensity.  $D_{5-75}$  ranges between 0.48 s to 89.29 s, with a mean of about 9.2 s. (Another duration measure,  $D_{5-95}$ , was also considered in the residual analysis). The distributions of  $M$ ,  $R_{RUP}$ ,  $V_{S30}$ , and  $D_{5-75}$  for our selected database of vertical ground motions are shown in Figure 2 as normalized frequency diagrams. The  $V_{S30}$  value is

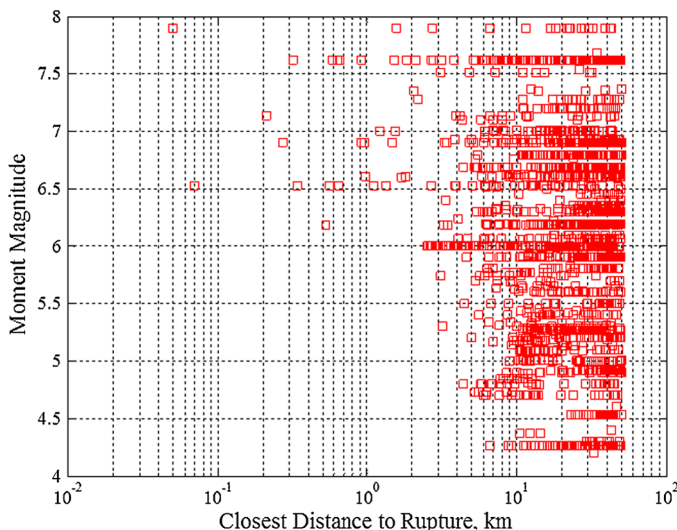


**Figure 1.** Magnitude-distance distribution of the selected database.

unknown for a few recordings; hence, the corresponding vertical axis in Figure 2 shows a smaller number of data points. The only visible difference compared to similar diagrams for the horizontal component is in the duration of motion. In general,  $D_{5-75}$  is slightly higher for the vertical component. ( $D_{5-75}$  for the horizontal motion varies between 0.25 s and 59.32 s, with a mean of about 7.5 s as reported in Rezaeian et al. 2014.)

In the literature, various terminologies and symbols are used for the damping scaling factor. We follow the notation used in Rezaeian et al. (2014) and define the damping scaling factor (DSF) as

$$DSF = \frac{PSA_{\beta\%}}{PSA_{5\%}} \quad (1)$$

where  $\beta$  represents the damping ratio of interest, and  $PSA$  denotes the elastic pseudo-spectral acceleration of the vertical ground motion at a damping ratio indicated in the subscript. The DSF is calculated according to Equation 1 for each record in the database at all 11 damping ratios and at the 21 spectral periods considered in the NGA projects:  $T = 0.01$  s, 0.02 s, 0.03 s, 0.05 s, 0.075 s, 0.1 s, 0.15 s, 0.2 s, 0.25 s, 0.3 s, 0.4 s, 0.5 s, 0.75 s, 1 s, 1.5 s, 2 s, 3 s, 4 s, 5 s, 7.5 s, and 10 s.

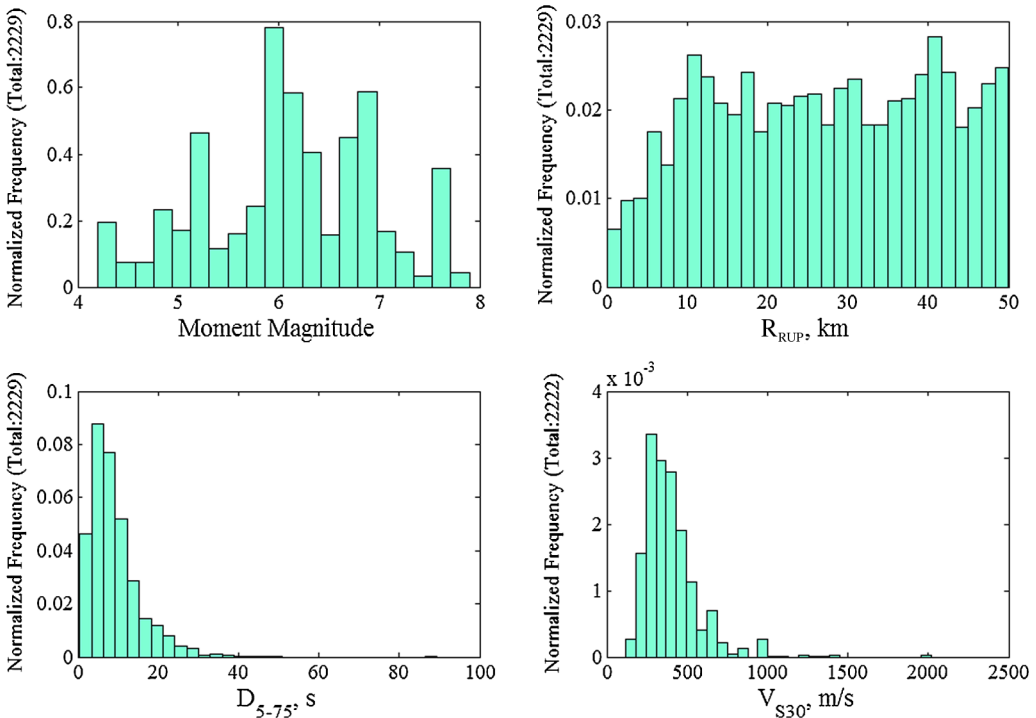


**Figure 2.** Distributions of parameters in the selected database.

Some studies (e.g., [Lin and Chang 2003](#)) argue that the absolute spectral acceleration (SA) should be used instead of the pseudo-spectral acceleration (PSA) to calculate the DSF. The reason is that the DSF calculated using PSA is in fact derived from the spectral displacement (SD),  $DSF = (SD_{\beta\%}) / (SD_{5\%}) = (PSA_{\beta\%}) / (PSA_{5\%})$ , and therefore, the use of it to reduce design forces is inappropriate. PSA approximation of SA simply neglects damping forces, which causes significant differences between PSA and SA at high damping ratios and long periods. These studies, which thus far have been specific to the horizontal ground motion, show significant differences between  $(PSA_{\beta\%}) / (PSA_{5\%})$  and  $(SA_{\beta\%}) / (SA_{5\%})$ , especially for  $\beta > 10\%$  and  $T > 0.15$  s. On the other hand, [Cameron and Green \(2007\)](#) provide a discussion on why the use of PSA-based DSF is valid for base isolated structures and structures with damping devices, where the structural system does not need to resist the entire induced inertial forces (only the part not resisted by the isolation or damping system), and for inelastic structures designed per the substitute structure method, where the design is based on a targeted maximum displacement. Given that the relatively recent engineering practice is being driven toward displacement-based design, we follow Equation 1 and use PSA to calculate the DSF. Additionally, the purpose of this study is to develop a model to be applied to PSA-based GMPEs, which makes the definition in Equation 1 appropriate. We acknowledge that at 5% damping, PSA approximately equals SA and consequently their GMPEs would be similar. However, PSA values begin to deviate radically from SA values at high damping ratios, approximately beyond 20% ([Chopra 2012](#)), and caution should be taken on selection of appropriate structural analysis techniques if damping ratios as high as 30% are used. This is likely the reason that many existing models have limited their maximum target damping ratio to 20% of critical.

## MODEL DEVELOPMENT

Our goal is to develop a predictive equation of the following generic form

$$\ln(DSF) = \mu(\beta, T, \text{earthquake, site}; \mathbf{b}) + \varepsilon \quad (2)$$

where  $\mu$  represents the mean of  $\ln(DSF)$ , which is a function of the damping ratio  $\beta$ , the spectral period  $T$ , and various earthquake and site characteristics such as earthquake magnitude, source-to-site distance, and site conditions;  $\mathbf{b}$  is the vector of regression coefficients; and  $\varepsilon$  represents the error term that is assumed to be normally distributed with zero mean and standard deviation  $\sigma$ .

In [Rezaeian et al. \(2014\)](#), we developed a model for the DSF of the horizontal ground motion, denoted hereafter as  $DSF_H$ .  $DSF_H$  was assigned a lognormal distribution and its predictive equation followed the form given in Equation 2 with predictor variables  $\beta$ ,  $\mathbf{M}$ , and  $R_{RUP}$ , and the regression coefficients given at the 21 NGA periods. In this study, after statistical data analysis, we assign also a lognormal distribution to the random variable  $DSF_V$ , where subscript  $V$  denotes the vertical ground motion. Furthermore, after scrutinizing our database of vertical ground motions, we observe that the general trends seen between  $DSF_V$  and various predictor variables are similar to what was observed for  $DSF_H$ . Namely, systematic patterns with damping ratio and vibration period, strong dependence on duration and magnitude, a weaker but relatively significant dependence on distance, and a negligible dependence on site conditions are observed. A step-by-step regression procedure and study

of residual diagnostic plots lead to selection of the functional form and identification of the model coefficients for  $DSF_V$ . More details are provided in the following.

**DISTRIBUTION OF DSF**

Traditionally, a lognormal distribution is assumed for ground motion intensity measures (i.e., PSA) at specified earthquake and site characteristics (e.g., given earthquake magnitude, source-to-site distance, etc.). If PSA is lognormally distributed, then  $\ln(PSA)$  follows a normal distribution. Following Equation 1,

$$\ln(DSF_V) = \ln(PSA_{\beta\%}) - \ln(PSA_{5\%}) \tag{3}$$

where each term on the right-hand side is assumed to be normally distributed. It is well-known that the linear combination of independent normally distributed random variables is normal. Therefore, if PSAs at two different damping ratios were independent variables, then it would be logical to assume a lognormal distribution for the  $DSF_V$ . But because PSA values at two different damping ratios can be dependent, we investigate the possibility that the  $DSF_V$  follows a lognormal distribution independently by statistical analysis of our available data.

At a specified  $T$  and  $\beta$ , we find the data for the  $DSF_V$  to be well represented by a log-normal distribution (i.e.,  $\ln(DSF_V)$  is normally distributed). Figure 3 shows example plots at

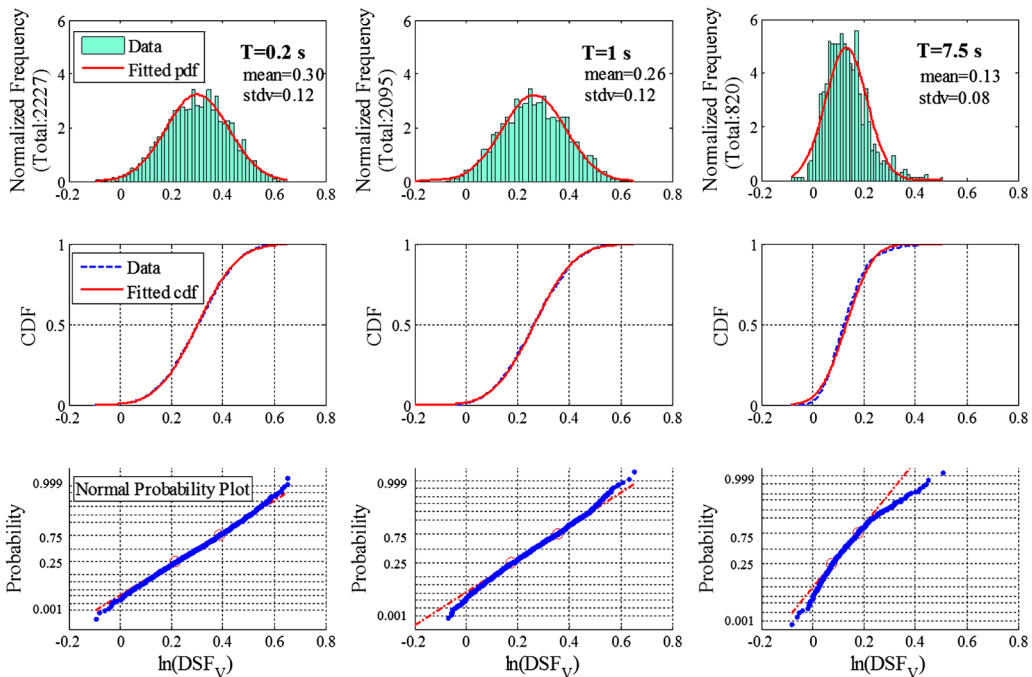


**Figure 3.** Distribution of  $\ln(DSF_V)$  at specified periods and  $\beta = 2\%$ .

$\beta = 2\%$  and  $T = 0.2$  s, 1 s, and 7.5 s. The top row shows the normalized frequency diagrams of  $\ln(DSF_V)$ . The normal distribution for each period is estimated by the method of moments and the resulting probability density function (PDF) is superimposed on the figure. Furthermore, the cumulative distribution function (CDF) of the fitted distribution is plotted along with the empirical CDF of data in the second row of Figure 3. The normal probability plots are shown in the bottom row of Figure 3, where the data within the first and third quartiles (marked by hollow circles) follow a straight line, thus confirming that the data for  $\ln(DSF_V)$  could follow a normal distribution. By visual inspection of histograms, examining the fit to the empirical CDF, and scrutinizing the normal probability plots at specified  $T$  and  $\beta$  values, we graphically assess the distribution of data and conclude that the  $\ln(DSF_V)$  data are representative of the normal distribution with a better fit at shorter periods (e.g., compare the plots at 0.2 s and 7.5 s in Figure 3). These results are typical for all periods and damping ratios with the exception of two scenarios: (1) at very short  $T$  and very low  $\beta$ , and (2) at very short  $T$  and very high  $\beta$  (examples are shown in Rezaeian et al. 2012). The  $DSF_V$  can be reasonably assumed a lognormal random variable for the purposes of this study at a specified  $T$  and  $\beta$ ; we do not see the need for any further hypothesis testing. Similar results were observed for  $DSF_H$ .

In the literature (see Introduction),  $DSF$  and  $\ln(DSF)$  have been inconsistently used on the left-hand side of Equation 2 (typically for the horizontal ground motion).  $DSF$  following a lognormal distribution supports the use of  $\ln(DSF)$  in Equation 2; assuming normal distribution of the error term leads to normal distribution of the response variable at specified values of earthquake and site characteristics. Choosing a suitable distribution for the response variable in the regression analysis could be an important factor when studying the symmetry of the residual diagnostic plots. Additionally, the choice of  $\ln(DSF)$  as the response variable in the regression analysis implies that the proposed model for  $\mu$  is for the median  $DSF$ .

## PREDICTOR VARIABLES

Based on the definition of the  $DSF$  and the strong dependence of  $PSA$  on  $T$ , the most obvious predictor variables are the damping ratio and spectral period. Figures 4 and 5 show the systematic patterns that exist between  $DSF_V$  and these two variables. In these figures, the data is divided by three magnitude bins (i.e.,  $M$  5 to  $M$  6,  $M$  6 to  $M$  7, and greater than  $M$  7). Furthermore, separate plots are presented for distances less than 50 km (selected database for regression analysis) and greater than 50 km (the remainder of records in the NGA-West2 database for moderate to large magnitude events). Similar to  $DSF_H$  (Rezaeian et al. 2014), the dependence on  $T$  is weak between 0.2 s to 2 s for  $\beta \geq 2\%$ , but there is a strong dependence outside this period range until  $DSF_V$  approaches unity for very short and very long  $T$  as expected. This is expected because the forces in a very stiff or a very flexible structure are relatively independent of the damping ratio. One can also explain this phenomenon due to the  $PSA$  approaching the peak ground acceleration at very short periods, and the  $SD$  approaching the peak ground displacement at very long periods; both of which are independent of the damping ratio. The dependence on  $T$  is much stronger for  $\beta \leq 1\%$ . Figures 4 and 5 also show the influence of magnitude and distance on  $DSF_V$ . These two variables were used in the model of  $DSF_H$  to capture the strong dependence on the duration of motion. In general, as  $M$  increases, the  $DSF$  decreases for  $\beta > 5\%$  at long periods, but a general increase

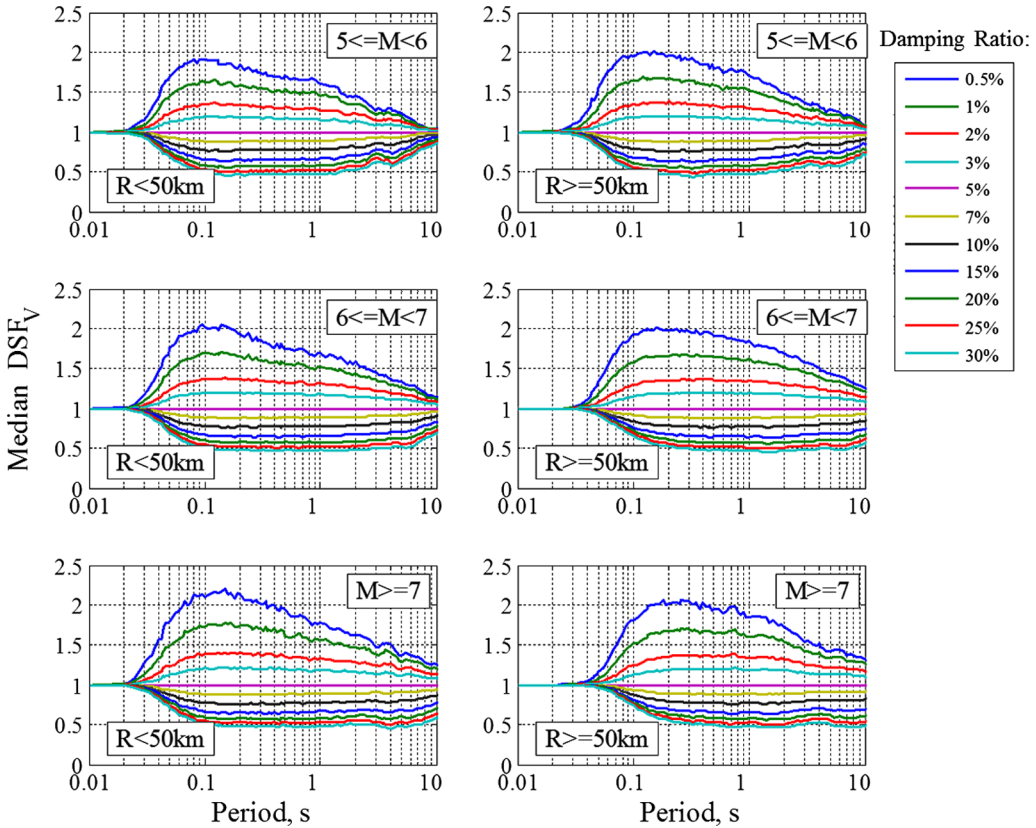


**Figure 4.** Median  $DSF_V$  versus period plotted for different magnitude-distance bins.

in the  $DSF$  is observed for  $\beta < 5\%$ . Also, a consistent deviation from unity at long periods is observed as distance increases.

Duration of motion has a strong influence on  $DSF_V$  because the number of energy dissipating cycles that increase with duration of motion can be influential on the equivalent viscous damping. Figure 6 shows the scatter plot of  $DSF_V$  in our selected database versus  $D_{5-75}$  at  $T = 1$  s for  $\beta = 2\%$  and  $20\%$ . A fitted line (using simple least squares regression) is superimposed on the figure only for visual purposes to show the linear correlation between  $DSF_V$  and  $\log(D_{5-75})$ . Dependence of  $DSF_V$  on  $D_{5-75}$  is less pronounced than that of  $DSF_H$ . Similar dependence is seen with  $D_{5-95}$ . Despite its strong influence on  $DSF$  relative to other variables, explicit inclusion of duration in the model is not ideal in practice because duration is generally not specified as part of a seismic design scenario. Therefore, we follow the approach we took in modeling  $DSF_H$  and capture the effects of duration on  $DSF_V$  by inclusion of both magnitude and distance in the model. In general, we expect to see a strong positive correlation between duration and magnitude, and a moderate positive correlation between duration and distance (e.g., Bommer et al. 2009). This statement is supported by our data. Similar to the observed patterns with  $D_{5-75}$  (e.g., Figure 6), we see that

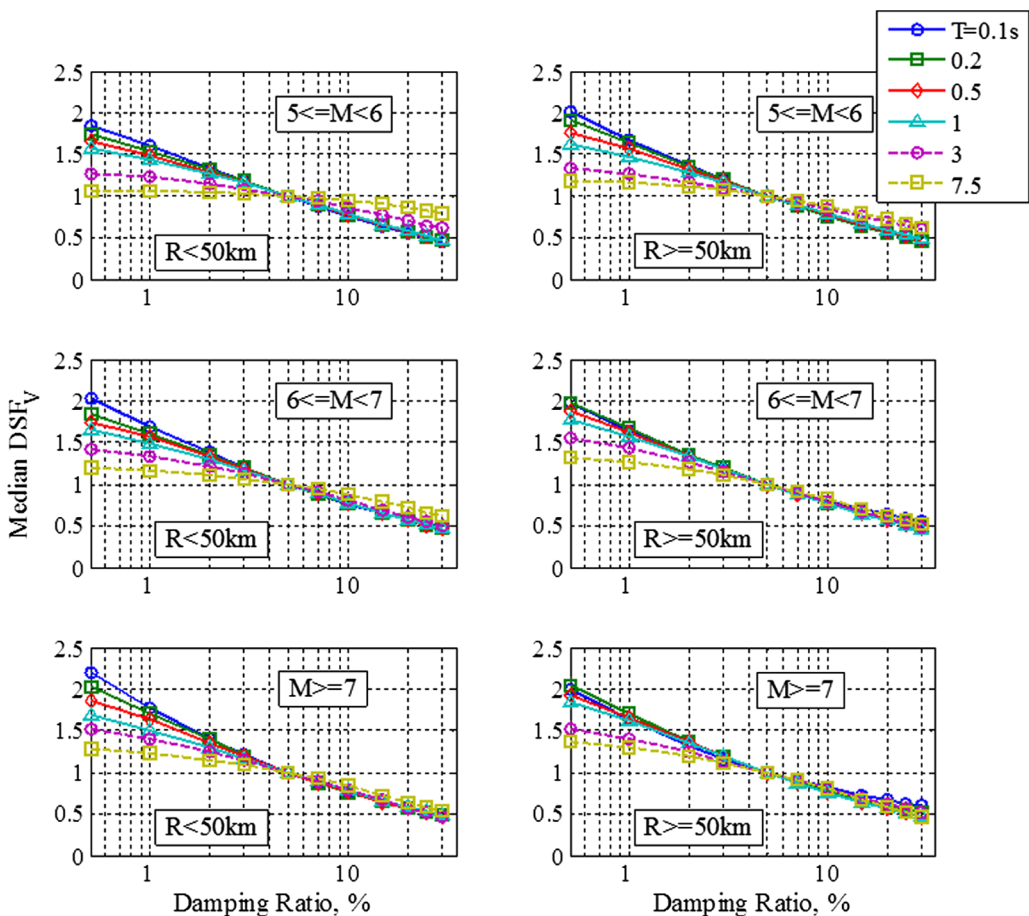


Figure 5. Median  $DSF_V$  versus damping ratio plotted for different magnitude-distance bins.

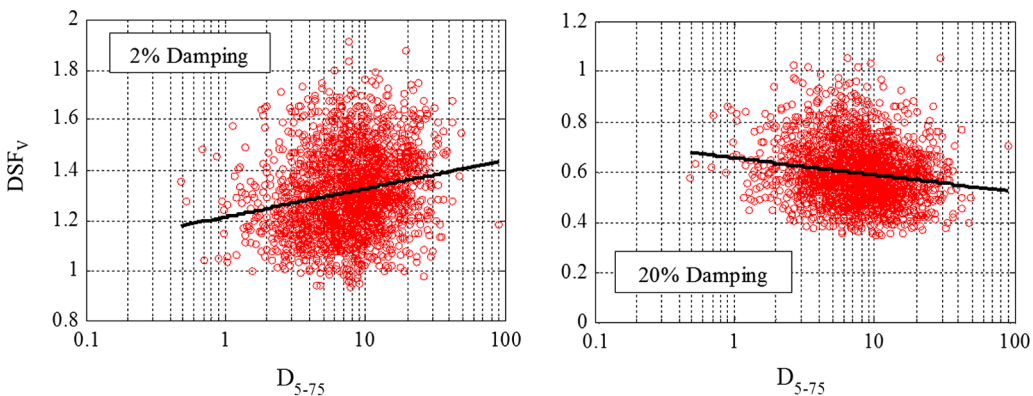
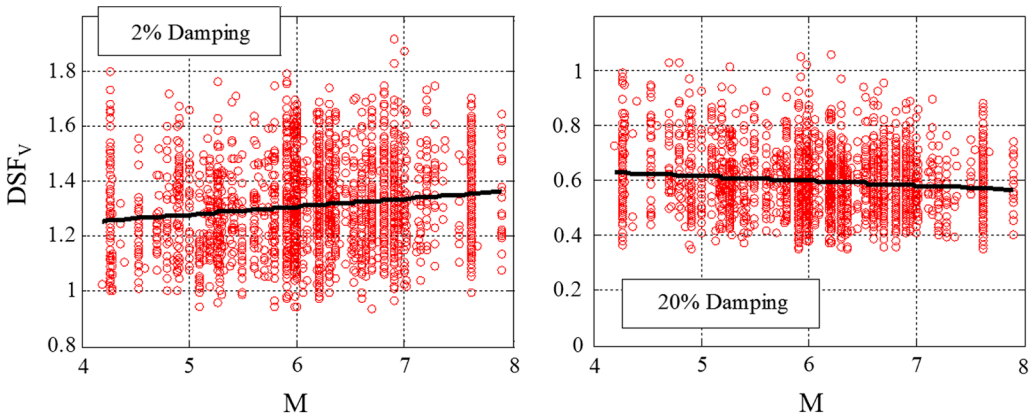


Figure 6. Influence of duration on  $DSF_V$  at  $T = 1$  s for records in the selected database.



**Figure 7.** Influence of magnitude on  $DSF_V$  at  $T = 1$  s for records in the selected database.

$DSF_V$  increases with  $M$  if  $\beta < 5\%$  and decreases if  $\beta > 5\%$ . This dependence on  $M$  is relatively strong (e.g., Figure 7). Similar patterns, but much weaker, are observed with  $R_{RUP}$  (e.g., Figure 8). Fitted lines are superimposed on each plot in Figures 7 and 8 to visually show the linear dependence. The patterns observed in Figures 7 and 8 are slightly weaker than those observed for  $DSF_H$ .

We investigate the influence of shallow site conditions by examining the dependence of  $DSF_V$  on  $V_{S30}$ . Similar to  $DSF_H$ , we find this dependence to be negligible. This is consistent with results found in the literature. For example, Malhotra (2006) also reported statistically insignificant differences between rock and soil sites. Additionally, the influence of sediment depth is examined by scrutinizing the residual plots of the model proposed in the next section versus available data for  $Z_{1.0}$  and  $Z_{2.5}$ , which respectively represent the depth to the 1.0 and 2.5 km/s shear-wave velocity horizons. No dependence is observed.

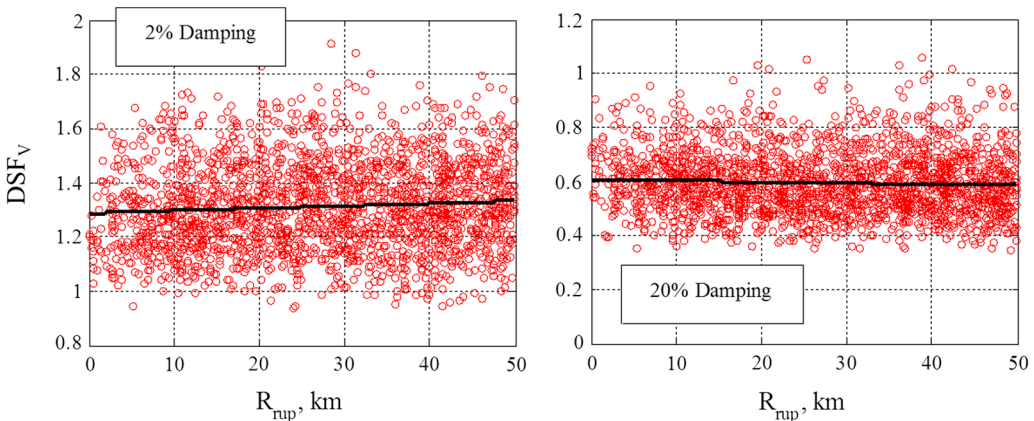


**Figure 8.** Influence of distance on  $DSF_V$  at  $T = 1$  s for records in the selected database.

## THE PROPOSED MODEL

We carry out a multistep least squares regression process, which is described in detail in Rezaeian et al. (2012) and summarized in Rezaeian et al. (2014).  $\mathbf{M}$  and  $R_{RUP}$  are selected as the predictor variables; then, the constant term and the coefficients of the magnitude and distance terms are expressed in terms of  $\beta$  at each specified period. The final model has a functional form the same as that of  $DSF_H$

$$\begin{aligned} \ln(DSF_V) = & b_0 + b_1 \ln(\beta) + b_2(\ln(\beta))^2 \\ & + [b_3 + b_4 \ln(\beta) + b_5(\ln(\beta))^2]\mathbf{M} \\ & + [b_6 + b_7 \ln(\beta) + b_8(\ln(\beta))^2] \ln(R_{RUP} + 1) \\ & + \varepsilon \end{aligned} \quad (4)$$

where  $\beta$  is the damping ratio as a percentage;  $R_{RUP}$  is in km;  $b_i$ ,  $i = 0, \dots, 8$ , are period-dependent regression coefficients given in Table 1; and  $\varepsilon$  is the error term. The standard deviation of  $\varepsilon$ , which represents the logarithmic standard deviation of  $DSF_V$ , shows a strong dependence on the damping ratio that can be captured by the following equation, which has the same functional form as the model for horizontal component

$$\sigma_{\ln(DSF_V)} = |a_0 \ln(\beta/5) + a_1(\ln(\beta/5))^2| \quad (5)$$

where  $a_0$  and  $a_1$  are period-dependent coefficients also given in Table 1. In Figures 9 and 10, the regression coefficients are plotted against period for the vertical ground motion. The corresponding plots for the horizontal ground motion, RotD50, from Rezaeian et al. (2014) are superimposed on these figures for comparison. Observe that the overall shape of a coefficient plotted versus period is similar for both vertical and horizontal components, but with a shift in the period. This shift is more obvious around 0.1 s. Smoothing of the model coefficients with respect to period is not necessary because the resulting  $DSF_V$  and, therefore, the scaled GMPE are smooth with respect to  $T$ . As an example, Figure 11a plots the predicted  $DSF_V$  according to Equation 4 for  $\mathbf{M} = 7$  and  $R_{RUP} = 10$  km. Figure 11b shows the predicted standard deviation according to Equation 5, which is independent of  $\mathbf{M}$  and  $R_{RUP}$ .

Figures 12 and 13 show the variation of  $DSF_V$  with magnitude and distance for several damping ratios. Figure 12 plots the predicted  $DSF_V$  at various magnitudes for  $R_{RUP} = 10$  km, whereas Figure 13 plots the same measure at various distances for  $\mathbf{M} = 7$ . Similar to  $DSF_H$  (Rezaeian et al. 2014), the variation with magnitude and distance is sensitive to the damping ratio. Much more variation is seen at 0.5% and 30% damping ratios compared to 3 and 7% damping ratios. In general, the variation with magnitude and distance is negligible at shorter periods and greater at longer periods. For  $DSF_V$ , there is usually a period range where we see almost no variation with magnitude, e.g., 0.2–0.7 s at a 20% damping ratio. Before and after this period range, the direction of the dependence between  $DSF_V$  and  $\mathbf{M}$  changes (i.e.,  $DSF_V$  increases with  $\mathbf{M}$  for periods less than 0.2 s but decreases with  $\mathbf{M}$  for periods greater than 0.7 s). This range reduces to just one period when it comes to the variation with  $R_{RUP}$  (see Figure 13).

Figure 14a compares the proposed model at a magnitude of 6.5 and 20 km distance with the median  $DSF_V$  calculated from records in a magnitude-distance bin of  $6 \leq \mathbf{M} \leq 7$  and  $0 \leq R_{RUP} < 50$  km. There is a good overall agreement between the data and the proposed

**Table 1.** Regression coefficients for the vertical damping scaling factor  $DSF_V$ 

$T$ (s)	$b_0$	$b_1$	$b_2$	$b_3$	$b_4$	$b_5$	$b_6$	$b_7$	$b_8$	$a_0$	$a_1$
0.01	5.82E-03	-3.31E-03	-3.64E-04	-3.81E-04	2.15E-04	2.92E-05	-1.82E-03	1.54E-03	-2.48E-04	-6.15E-03	5.21E-04
0.02	1.36E-01	-8.77E-02	1.65E-03	-1.02E-02	6.91E-03	-2.83E-04	-1.23E-02	6.98E-03	3.60E-04	-4.50E-02	3.16E-03
0.03	3.49E-01	-1.94E-01	-1.19E-02	-1.61E-02	6.48E-03	1.95E-03	-2.59E-02	1.22E-02	2.19E-03	-1.06E-01	3.16E-03
0.05	4.34E-01	-1.68E-01	-6.08E-02	-1.15E-03	-1.01E-02	6.59E-03	-1.37E-02	-3.18E-03	6.97E-03	-1.47E-01	-8.28E-03
0.075	3.48E-01	-6.40E-02	-9.47E-02	1.69E-02	-2.37E-02	8.31E-03	6.22E-03	-1.97E-02	9.83E-03	-1.39E-01	-9.96E-03
0.1	3.06E-01	-3.80E-02	-9.44E-02	2.63E-02	-2.96E-02	8.20E-03	1.14E-02	-1.80E-02	6.93E-03	-1.34E-01	-1.02E-02
0.15	1.87E-01	6.67E-02	-1.16E-01	4.32E-02	-4.50E-02	1.15E-02	1.66E-02	-1.73E-02	4.82E-03	-1.23E-01	-6.66E-03
0.2	1.86E-01	4.16E-02	-9.66E-02	3.55E-02	-3.56E-02	8.37E-03	2.73E-02	-2.37E-02	4.13E-03	-1.22E-01	-6.52E-03
0.25	1.21E-01	7.76E-02	-9.75E-02	4.13E-02	-3.96E-02	8.98E-03	3.10E-02	-2.22E-02	1.97E-03	-1.20E-01	-5.99E-03
0.3	1.41E-01	5.39E-02	-8.91E-02	3.79E-02	-3.61E-02	7.91E-03	2.76E-02	-1.85E-02	1.02E-03	-1.22E-01	-5.78E-03
0.4	1.72E-01	1.29E-02	-7.08E-02	2.97E-02	-2.58E-02	4.42E-03	2.93E-02	-2.13E-02	1.05E-03	-1.20E-01	-5.74E-03
0.5	2.21E-01	-3.86E-02	-6.00E-02	2.18E-02	-1.90E-02	3.21E-03	2.72E-02	-1.64E-02	-2.29E-04	-1.23E-01	-6.08E-03
0.75	1.68E-01	-2.35E-02	-5.40E-02	2.49E-02	-1.57E-02	6.34E-04	3.10E-02	-2.21E-02	2.01E-03	-1.22E-01	-6.75E-03
1	8.65E-02	2.28E-02	-5.28E-02	3.47E-02	-2.11E-02	4.55E-04	3.53E-02	-2.43E-02	1.75E-03	-1.24E-01	-8.33E-03
1.5	-3.62E-02	7.02E-02	-3.20E-02	4.82E-02	-2.57E-02	-2.44E-03	3.63E-02	-2.24E-02	2.93E-04	-1.25E-01	-1.04E-02
2	-8.29E-02	9.13E-02	-2.57E-02	5.37E-02	-2.64E-02	-4.34E-03	3.16E-02	-2.30E-02	2.38E-03	-1.22E-01	-1.11E-02
3	-2.26E-01	1.21E-01	1.05E-02	6.50E-02	-2.59E-02	-8.86E-03	3.45E-02	-2.00E-02	-9.44E-04	-1.16E-01	-1.29E-02
4	-4.08E-01	2.02E-01	3.12E-02	8.61E-02	-3.44E-02	-1.19E-02	4.15E-02	-2.23E-02	-2.25E-03	-1.11E-01	-1.63E-02
5	-2.54E-01	1.11E-01	2.96E-02	6.37E-02	-2.13E-02	-1.15E-02	2.86E-02	-1.34E-02	-2.90E-03	-1.07E-01	-1.68E-02
7.5	-4.41E-01	1.73E-01	6.26E-02	7.73E-02	-2.58E-02	-1.39E-02	3.84E-02	-1.44E-02	-5.92E-03	-9.36E-02	-1.63E-02
10	-3.95E-01	1.23E-01	7.79E-02	7.10E-02	-2.12E-02	-1.43E-02	2.13E-02	-4.42E-03	-6.15E-03	-8.17E-02	-1.53E-02

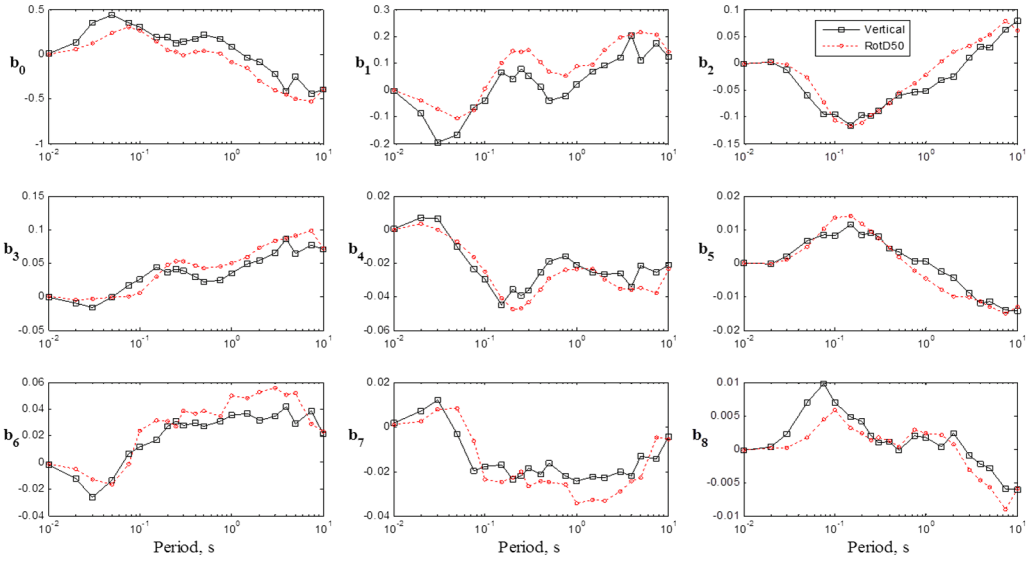


**Figure 9.** Model coefficients for  $DSF_V$  (vertical), compared to those for  $DSF_H$  (RotD50).

model. As discussed in the introduction, very few models exist in the literature for  $DSF_V$ . The model by [Malhotra \(2006\)](#) is not directly comparable to the proposed model because it depends on peak ground acceleration, peak ground velocity, and peak ground displacement to construct the design response spectra at various damping ratios. The model by [Abrahamson and Silva \(1996\)](#) is compared to the proposed model in [Figure 14b](#). This model is a function of  $M$ , but not  $R_{RUP}$ , and is applicable to  $T = 0.02 - 5$  s. It is calculated and plotted only at select periods, and we linearly interpolated the model in between. In [Figure 14b](#), the proposed model is plotted for  $M = 6.5$ ,  $R_{RUP} = 20$  km, and all 11 damping ratios from 0.5 to 30% and the [Abrahamson and Silva \(1996\)](#) model is plotted for  $M = 6.5$  and  $\beta = 0.5\%$ , 1%, 2%, 3%, 5%, 7%, 10%, 15%, and 20%. Except for very low damping, where the peak is at a shorter period in our model, there is a relatively good agreement between the two models.

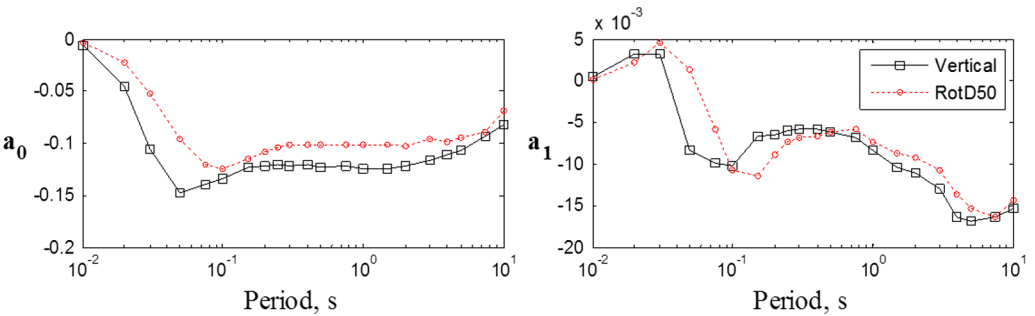


**Figure 10.** Model coefficients for the logarithmic standard deviation of  $DSF_V$  (vertical), compared to those for  $DSF_H$  (RotD50).

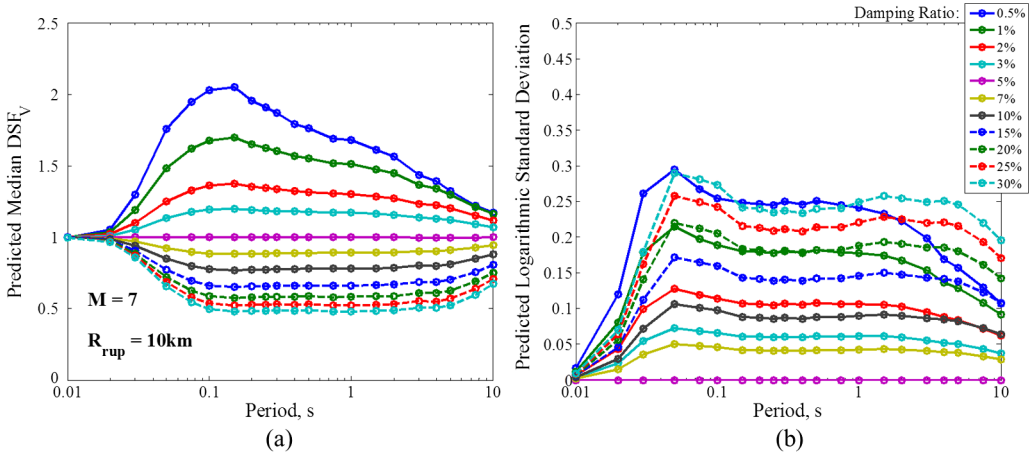


**Figure 11.** Predicted (a) median  $DSF_V$  according to Equation 4 at a given magnitude and distance, and (b) logarithmic standard deviation according to Equation 5.

**Analysis of Residuals**

One of the classical data exploration techniques is the analysis of residuals. We define the model residual as the difference between the observed and predicted (i.e., calculated) values of  $\ln(DSF)$ . In the model-building process, we examined the residuals at each step to assess the adequacy of the selected functional form. We inspected the residuals to examine departures from normality. Furthermore, the plots of the residuals versus explanatory variables (including those variables that were not included in the model, e.g., duration, site conditions)

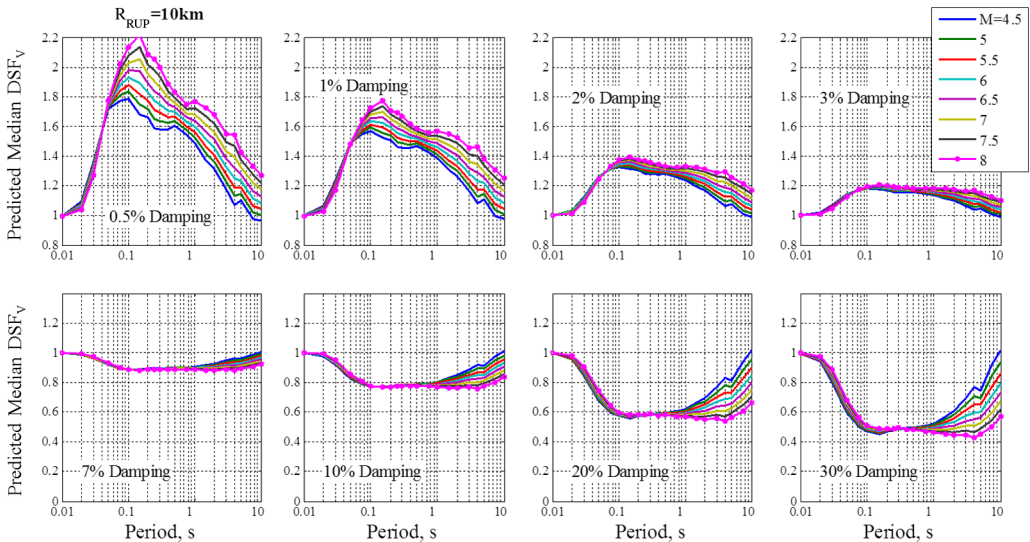


**Figure 12.** Variation of median  $DSF_V$  with magnitude at 10 km distance.

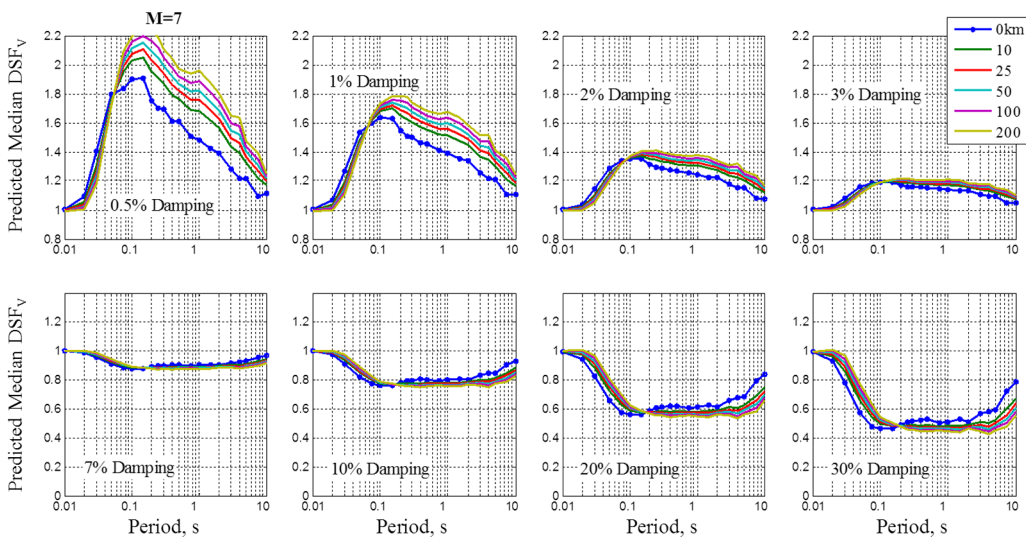


Figure 13. Variation of median  $DSF_V$  with distance at magnitude of 7.0.

were examined for symmetry around zero and for any systematic trends. Figure 15 shows examples of residual diagnostic plots for the proposed model in Equation 4 at  $T = 0.2$  s. Only data with distances less than 50 km are plotted. Figure 15a shows the dependence of the residuals on the damping ratio. Figures 15b–g show the dependence on magnitude,

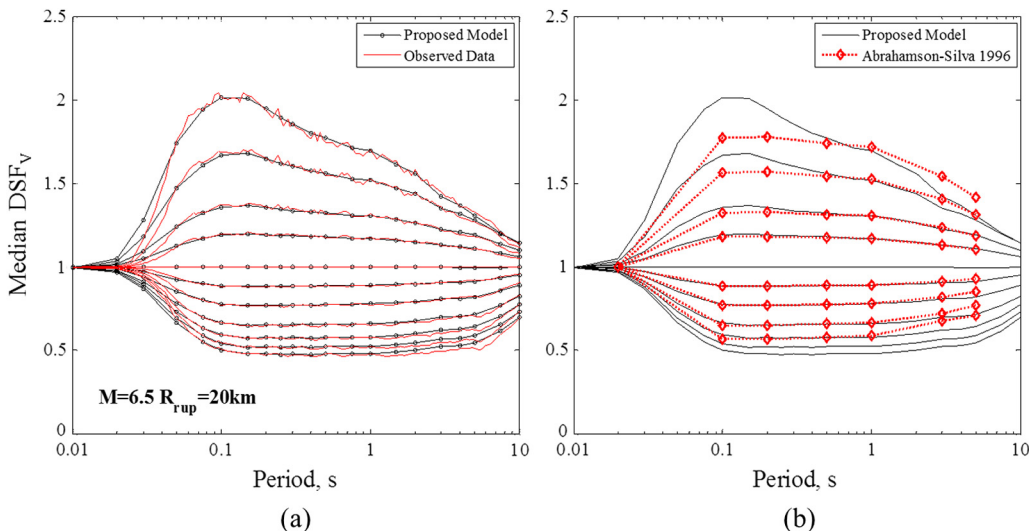
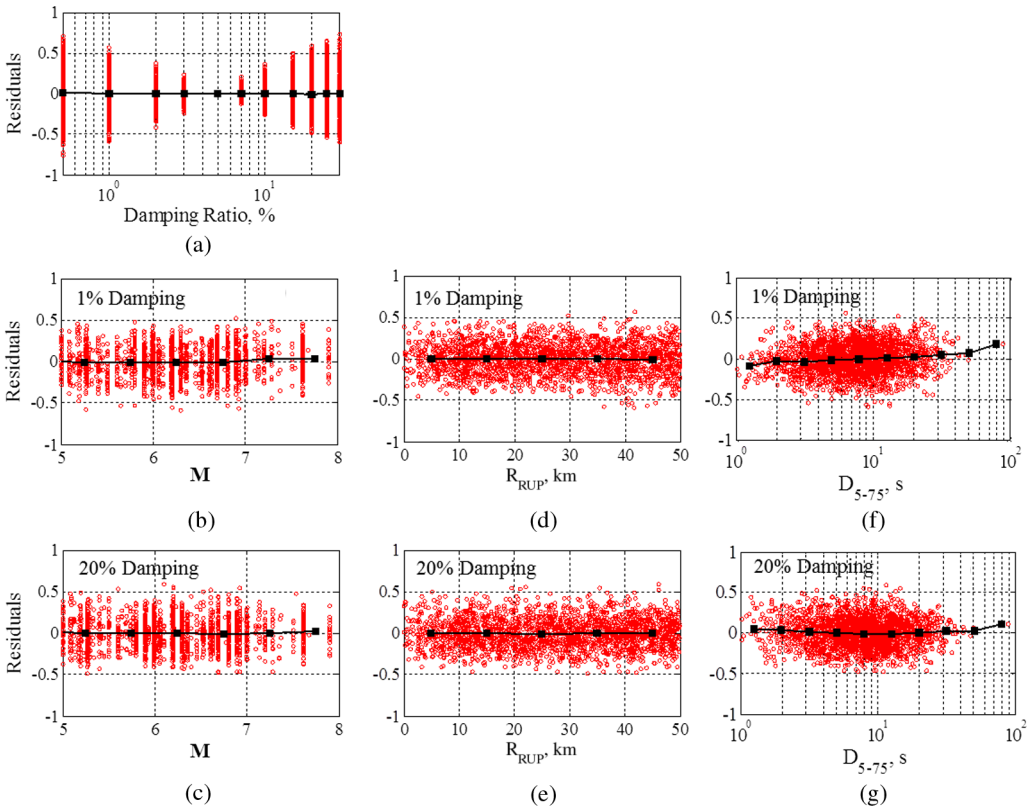


Figure 14. The proposed model is plotted for  $M = 6.5$  and  $R_{RUP} = 20$  km at all 11 damping ratios from 0.5% to 30%. (a) Data for magnitude-distance bin of  $6 \leq M \leq 7$  and  $0 \leq R_{RUP} < 50$  km is superimposed. (b) Abrahamson and Silva (2006) model is superimposed for  $M = 6.5$  at  $\beta = 0.5\%$ , 1%, 2%, 3%, 7%, 10%, 15%, 20%.



**Figure 15.** Residuals plotted against predictor variables at  $T = 0.2$  s using data with  $R_{RUP} < 50$  km.

distance, and duration at 1% and 20% damping ratios. In each plot, a black line indicates the average values of residuals over equally spaced bins of data for visual inspection of patterns. Similar plots for other explanatory variables, periods, damping ratios, and distance ranges (e.g., beyond 50 km) are examined to confirm the general validity of the model. The residual plots for data with  $50 \leq R_{RUP} < 200$  km reveal an insignificant trend with the explanatory variables and we conclude that the model is applicable to distances up to 200 km. In [Rezaeian et al. \(2014\)](#), a maximum applicable distance of 200 km was also recommended; however, some NGA-West2 GMPEs were developed for a maximum distance of 300 km; thus, we examined the residual diagnostic plots and concluded that extrapolation of the models for both  $DSF_H$  and  $DSF_V$  up to a distance of 300 km are reasonable with the exception at very short periods (about less than 0.1 s).

### Standard Deviation of the Scaled Spectrum

Due to the small values of  $\sigma_{\ln(DSF)}$  relative to the standard deviation of the predicted 5% damped PSA,  $\sigma_{\ln(PSA_{5\%})}$ , the standard deviation of the scaled response spectrum, denoted  $\sigma_{\ln(PSA_{p\%})}$ , is mainly controlled by  $\sigma_{\ln(PSA_{5\%})}$ . Based on this premise, one can approximate

$\sigma_{\ln(PSA_{\beta\%})}$  by  $\sigma_{\ln(PSA_{5\%})}$ . For more accurate calculation of  $\sigma_{\ln(PSA_{\beta\%})}$ , an equation is presented in Rezaeian et al. (2014) that, in addition to  $\sigma_{\ln(PSA_{5\%})}$ , depends on  $\sigma_{\ln(DSF)}$  and the correlation coefficient between  $\ln(DSF)$  and  $\ln(PSA_{5\%})$ . Sample correlation coefficients were calculated in Rezaeian et al. (2012) for the horizontal components. Sample correlation coefficients for the vertical component have similar behavior with damping ratio and period as those for the horizontal component; that is, they tend to be very small at short periods and negative for  $\beta > 5\%$  with a high positive value of around 0.4 at very long  $T$  and  $\beta < 5\%$ .

### DSF FOR VERTICAL VERSUS HORIZONTAL

As previously mentioned the vertical component of ground motion has different characteristics than the horizontal component, these characteristics were outlined in the Introduction; consequently, differences between  $DSF_V$  and  $DSF_H$  are expected. In the previous section, plots of the model coefficients for the two components were compared in Figures 9 and 10. In this section, for a more direct comparison, Figure 16 shows plots of  $DSF_V$

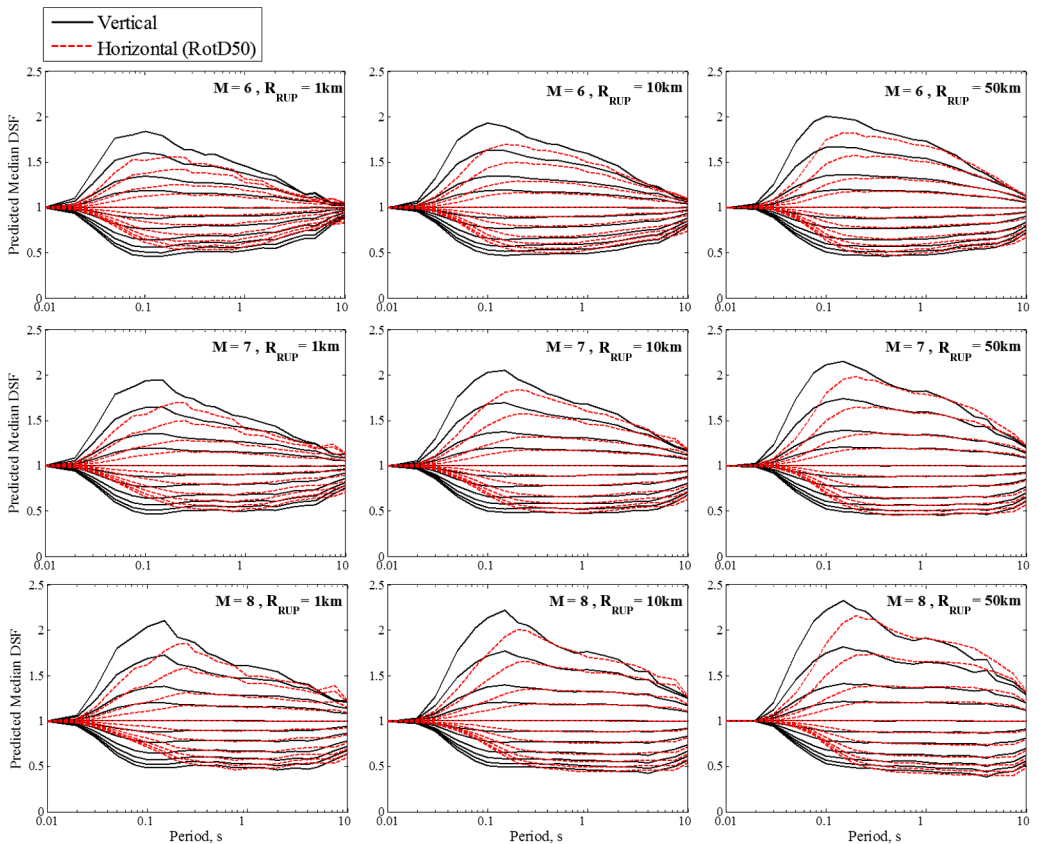


**Figure 16.** Comparison between predicted median  $DSF_V$  and  $DSF_H$  (i.e., calculated using the proposed models in this study) at  $M = 6, 7, 8$  and  $R_{RUP} = 1 \text{ km}, 10 \text{ km}, 50 \text{ km}$  for 11 damping ratios from 0.5% at the top to 30% at the bottom.

(according to the model presented in this paper) and  $DSF_H$  (according to the model proposed in Rezaeian et al. 2014 for RotD50) at selected values of  $M$  and  $R_{RUP}$ . The two models follow the same functional form but have different model coefficients. Each column in Figure 16 shows the variation of the DSF with magnitude at a specified distance, whereas each row shows the variation of the DSF with distance at a specified magnitude. In general, the peak is shifted toward shorter periods and is farther from unity for  $DSF_V$ . The most significant differences are seen at shorter periods, i.e.,  $T < 0.2$  s. These differences are likely due to the richer high-frequency contents of the vertical component.

The standard deviation versus period is plotted in Figure 17 at different damping ratios for the vertical and the horizontal components. Observe that the standard deviation for the vertical component is a little higher than what we see for the horizontal component, with a maximum of about 0.3. We suspect this effect is due to the “averaging” of the two horizontal components, which is expected to reduce the standard deviation compared to the single component used for vertical ground motion.

Two options are available to obtain vertical response spectra for damping ratios other than 5%. The premise of this paper is based on first obtaining the 5% damped vertical response spectra, then applying the  $DSF_V$  to transform them to other target damping ratios. An alternative approach is to first apply the  $DSF_H$  to the horizontal response spectra; then, use the V/H model for 5% damping to obtain the vertical spectra. The latter approach suffers from the lack of V/H models for damping ratios other than 5%, and consequently, it assumes that the V/H ratios derived using 5% damped spectral ordinates are applicable for other damping ratios. Figure 18 shows the median V/H for various damping ratios, using the records with distances less than 50 km that were used in this study. Observe that V/H varies

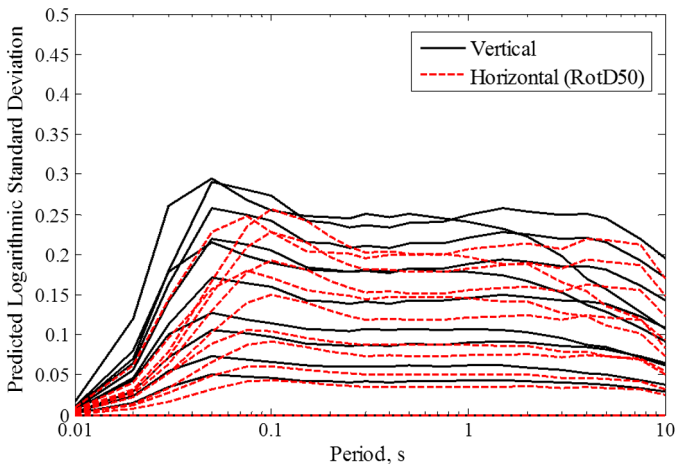


**Figure 17.** Comparison between the predicted standard deviation of  $DSF_V$  and  $DSF_H$  (i.e., calculated using the proposed models in this study). Only two line types are selected in this figure to emphasize the differences between vertical and horizontal components, legend for various damping ratios is according to Figure 11b.

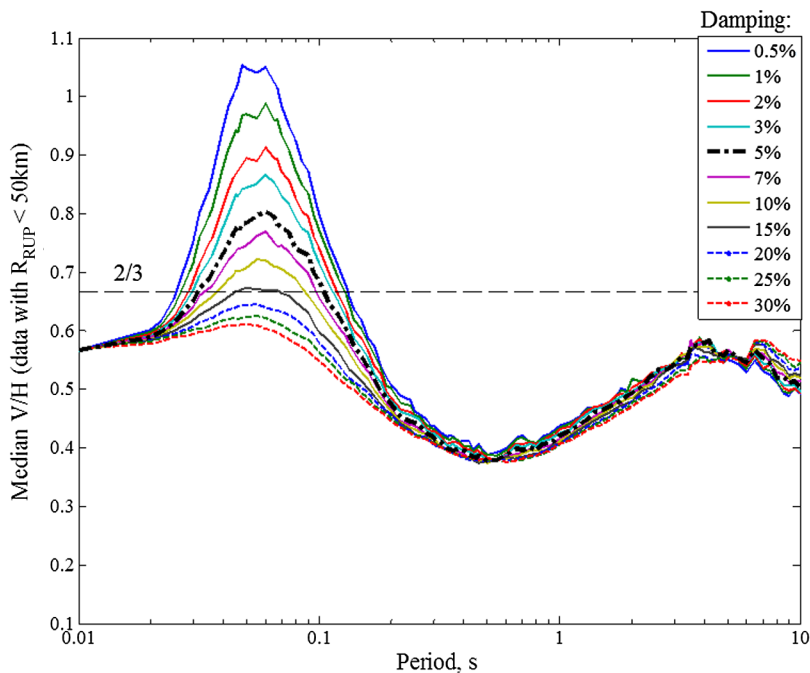


**Figure 18.** Median V/H, vertical to horizontal spectral ratio, for various damping levels using the database in this study with distances less than 50 km. RotD50 component is used to represent the horizontal motion.

substantially with damping ratio for periods between 0.02 s to 0.2 s. Therefore, one should exercise care if the latter method is used to obtain vertical response spectra.

## CONCLUSIONS

We empirically developed a new model for the damping scaling factor of the vertical component of ground motion,  $DSF_V$ . This model can be used to scale vertical elastic pseudo-spectral acceleration ordinates predicted at a 5% damping ratio to ordinates for other damping ratios from 0.5% to 30%. The database of recorded ground motions used to develop the model was a subset of the extensive NGA-West2 project database. We used 2,229 records from 218 earthquakes with distances of less than 50 km in the regression analysis. The validity of the resulting model for longer distances was examined by residual analysis of the remainder of records. We observed that the general trends seen between  $DSF_V$  and potential predictor variables—damping ratio, spectral period, duration, magnitude, distance, and site conditions—are similar to what was observed in [Rezaeian et al. \(2014\)](#) for the horizontal component scaling factor,  $DSF_H$ . Damping ratio was directly included in the model as a predictor variable. The strong influence of duration was captured by inclusion of both magnitude and distance in the model. The functional form is the same as that of  $DSF_H$  and is presented in Equation 4. The model coefficients are given in Table 1 for 21 spectral periods ranging from 0.01 s to 10 s. We decided that the influence of site conditions is

negligible and did not include them as predictor variables in our model. We also developed a model for the logarithmic standard deviation of  $DSF_V$ , which is a function of the damping ratio and spectral period and is presented in Equation 5 with coefficients given in Table 1. Finally, we highlighted the differences between  $DSF_V$  and  $DSF_H$  in Figures 16 and 17. In general, the median peak is shifted toward shorter periods and is more extreme (larger for damping ratios less than 5%, and smaller for damping ratios greater than 5%), and the standard deviation is slightly higher for  $DSF_V$ . The proposed  $DSF_V$  model is applicable to shallow crustal earthquakes in active tectonic regions for damping ratios from 0.5% to 30%, periods from 0.01 to 10 s, moment magnitudes between 4.5 and 8.0, and distances less than 300 km. Because the model was developed based on recorded data, it is independent of any specific ground motion prediction equation.

### ACKNOWLEDGMENTS

This study was sponsored by the Pacific Earthquake Engineering Research Center (PEER) and funded by the California Earthquake Authority, California Department of Transportation, and the Pacific Gas & Electric Company. Any opinions, findings, and conclusions or recommendations expressed in this material are those of the authors and do not necessarily reflect those of the above mentioned agencies. S. Rezaeian acknowledges the Natural Hazards Mission Area of the U.S. Geological Survey for support of her activities related to this study. We would like to thank all the NGA model developers and supporting researchers for their assistance and valuable feedback throughout this project. Special thanks are due Dr. Julian J. Bommer and other reviewers of this manuscript.

### REFERENCES

- Abrahamson, N. A., and Silva, W. J., 1996. *Empirical Ground Motion Models*, Section 4: Spectral scaling for other damping values, Report, Brookhaven National Laboratory.
- Abrahamson, N. A., and Silva, W. J., 1997. Empirical response spectral attenuation relations for shallow crustal earthquakes, *Seismological Research Letters* **68**, 94–127.
- Amirbekian, R. V., and Bolt, B. A., 1998. Spectral comparison of vertical and horizontal seismic strong ground motions in alluvial basins, *Earthquake Spectra* **14**, 573–595.
- Ancheta, T., Darragh, R., Stewart, J., Seyhan, E., Silva, W., Chiou, B., Woodell, K., Graves, R., Kottke, A., Boore, D., Kishida, T., and Donahue, J., 2013. *PEER NGA-West2 Database*, PEER Report 2013/03, Pacific Earthquake Engineering Research Center, Berkeley, CA.
- Aoi, S., Kunugi, T., and Fujiwara, H., 2008. Trampoline effect in extreme ground motion, *Science* **322**, 727–729.
- Beresnev, I. A., Nightengale, A. M., and Silva, W. J., 2002. Properties of vertical ground motions, *Bulletin of the Seismological Society of America* **92**, 3152–3164.
- Berge-Thierry, C., Cotton, F., Scotti, O., Griot-Pommer, D. A., and Fukushima, Y., 2003. New empirical response spectral attenuation laws for moderate European earthquakes, *Journal of Earthquake Engineering* **7**, 193–222.
- Bommer, J. J., Akkar, S., and Kale, O., 2011. A model for vertical-to-horizontal response spectral ratios for Europe and the Middle East, *Bulletin of the Seismological Society of America* **101**, 1783–1806.

- Bommer, J. J., Stafford, P. J., and Alarcon, J. E., 2009. Empirical equations for the prediction of the significant, bracketed and uniform duration of earthquake ground motion, *Bulletin of the Seismological Society of America* **99**, 3217–3233.
- Boore, D. M., 2010. Orientation-independent, non geometric-mean measures of seismic intensity from two horizontal components of motion, *Bulletin of the Seismological Society of America* **100**, 1830–1835.
- Boore, D. M., Watson-Lamprey, J., and Abrahamson, N. A., 2006. Orientation-independent measures of ground motion, *Bulletin of the Seismological Society of America* **96**, 1502–1511.
- Bozorgnia, Y., Abrahamson, N. A., Campbell, K. W., Rowshandel, B., and Shantz, T., 2012. NGA-West2: A comprehensive research program to update ground motion prediction equations for shallow crustal earthquakes in active tectonic regions, in *Proceedings, 15<sup>th</sup> World Conference on Earthquake Engineering*, Lisbon, Portugal. Paper Number 2572.
- Bozorgnia, Y., and Bertero, V. V., 2004. *Earthquake Engineering: From Engineering Seismology to Performance-Based Engineering*, CRC Press, Boca Raton, FL.
- Bozorgnia, Y., and Campbell, K. W., 2004. The vertical-to-horizontal response spectral ratio and tentative procedures for developing simplified V/H and vertical design spectra, *Journal of Earthquake Engineering* **8**, 175–207.
- Bozorgnia, Y., Mahin, S. A., and Brady, A. G., 1998. Vertical response of twelve structures recorded during the Northridge earthquake, *Earthquake Spectra* **14**, 411–432.
- Bozorgnia, Y., Niazi, M., and Campbell, K. W., 1995. Characteristics of free-field vertical ground motion during the Northridge earthquake, *Earthquake Spectra* **11**, 515–525.
- Building Seismic Safety Council (BSSC), 2009. *NEHRP Recommended Provisions for Seismic Regulations for New Buildings and other Structures*, FEMA P-750, Federal Emergency Management Agency, Washington, D.C.
- Campbell, K. W., 1985. Strong motion attenuation relations: A ten-year perspective, *Earthquake Spectra* **1**, 759–804.
- Campbell, K. W., 1997. Empirical near-source attenuation relationships for horizontal and vertical components of peak ground acceleration, peak ground velocity, and pseudo-absolute acceleration response spectra, *Bulletin of the Seismological Society of America* **68**, 154–176.
- Campbell, K. W., and Bozorgnia, Y., 2003. Updated near-source ground motion (attenuation) relations for the horizontal and vertical components of peak ground acceleration and acceleration response spectra, *Bulletin of the Seismological Society of America* **93**, 314–331.
- Comité Européen de Normalisation (CEN), 2004. *Eurocode 8: Design of Structures for Earthquake Resistance—Part 1: General Rules, Seismic Actions, and Rules for Buildings*, EN 1998-1:2004, Comité Européen de Normalisation, Brussels.
- Chopra, A. K., 2012. *Dynamics of Structures, Theory and Applications to Earthquake Engineering*, 4<sup>th</sup> Edition, Prentice Hall, Upper Saddle River, NJ.
- Elnashai, A. S., and Papazoglou, A. J., 1997. Procedure and spectra for analysis of RC structures subjected to strong vertical earthquake loads, *Journal of Earthquake Engineering* **1**, 121–155.
- Federal Emergency Management Agency (FEMA-356), 2000. *Prestandard and Commentary for the Seismic Rehabilitation of Buildings*, Washington, D.C.
- Gülerce, Z., and Abrahamson, N. A., 2011. Site-specific design spectra for vertical ground motion, *Earthquake Spectra* **27**, 1023–1047.
- Kempton, J. J., and Stewart, J. P., 2006. Prediction equations for significant duration of earthquake ground motions considering site and near-source effects, *Earthquake Spectra* **22**, 985–1013.

- Lin, Y. Y., and Chang, K. C., 2003. Study on damping reduction factor for buildings under earthquake ground motions, *Journal of Structural Engineering*, ASCE **129**, 206–214.
- Malhotra, P. K., 2006. Smooth spectra of horizontal and vertical ground motions, *Bulletin of the Seismological Society of America* **96**, 505–518.
- McGuire, R. K., Silva, W. J., and Costantino, C. J., 2001. *Technical Basis for Revision of Regulatory Guidance on Design Ground Motions: Hazard- and Risk-Consistent Ground Motion Spectra Guidelines*, Section 4.9: Estimation of spectra for other dampings, Report, NUREG/CR-6728. Prepared for Division of Engineering Technology, Office of Nuclear Regulatory Research, U.S. Nuclear Regulatory Commission, Washington, D.C.
- Mohraz, B., 1976. A study of earthquake response spectra for different geological conditions, *Bulletin of the Seismological Society of America* **66**, 915–935.
- Newmark, N. M., and Hall, W. J., 1982. *Earthquake Spectra and Design*, Monograph, Earthquake Engineering Research Institute, Oakland, CA.
- Niazi, M., and Bozorgnia, Y., 1991. Behavior of near-source peak horizontal and vertical ground motions over SMART-1 Array, Taiwan, *Bulletin of the Seismological Society of America* **81**, 715–732.
- Niazi, M., and Bozorgnia, Y., 1992. Behaviour of near-source vertical and horizontal response spectra at SMART-1 array, Taiwan, *Earthquake Engineering and Structural Dynamics* **21**, 37–50.
- Power, M., Chiou, B. S.-J., Abrahamson, N. A., Roblee, C., Bozorgnia, Y., and Shantz, T., 2008. An introduction to NGA, *Earthquake Spectra* **24**, 3–21.
- Rezaeian, S., Bozorgnia, Y., Idriss, I. M., Campbell, K., Abrahamson, N., and Silva, W., 2012. *Spectral Damping Scaling Factors for Shallow Crustal Earthquakes in Active Tectonic Regions*, PEER Report 2012/102, Pacific Earthquake Engineering Research Center, Berkeley, CA.
- Rezaeian, S., Bozorgnia, Y., Idriss, I. M., Campbell, K., Abrahamson, N., and Silva, W., 2014. Damping scaling factors for elastic response spectra for shallow crustal earthquakes in active tectonic regions: “Average” horizontal component, *Earthquake Spectra* **30**, 939–963.
- Rosenblueth, E., 1980. Characteristics of earthquakes, in E. Rosenblueth, editor, *Design of Earthquake Resistant Structures*, Wiley.
- Sadigh, K., Chang, C. Y., Egan, J. A., Makdisi, F., and Youngs, R. R., 1997. Attenuation relationships for shallow crustal earthquakes based on California strong motion data, *Seismological Research Letters* **68**, 180–189.
- Silva, W., 1997. Characteristics of vertical strong ground motions for applications to engineering design, in *Proceedings, FHWA/NCEER Workshop on the National Representation of Seismic Ground Motion for New and Existing Highway Facilities, Burlingame, CA*, Technical Report NCEER-97-0010, National Center for Earthquake Engineering Research, Buffalo, New York.
- Tezcan, J., and Piolatto, A., 2012. A probabilistic nonparametric model for the vertical-to-horizontal spectral ratio, *Journal of Earthquake Engineering* **16**, 142–157.
- Trifunac, M. D., and Lee, V. W., 1989. Empirical models for scaling pseudo relative velocity spectra of strong earthquake accelerations in terms of magnitude, distance, site intensity and recording site conditions, *Soil Dynamics and Earthquake Engineering* **8**, 126–144.
- Vanmarcke, E. H., 1976. Structural response to earthquakes, in *Seismic Risk and Engineering Decisions*, edited by C. Lomnitz and E. Rosenblueth, Elsevier Publishing Co., New York.

(Received 5 October 2012; accepted 16 October 2013)